The Korean Journal of Rheology,
Vol. 9, No. 4, December 1997 pp. 140-150

<연구논문>

일축방향으로 배향된 보강섬유층 내로의 비뉴톤성 유체의 수직방향 침투도

이재식* · 이재욱
서강대학교 화학공학과
(1997년 8월 12일 접수)

Transverse Permeability of Generalized Newtonian Fluids Through Unidirectional Fibrous Porous Media

Jae Shik Lee* and Jae Wook Lee
Department of Chemical Engineering, Sogang University, Seoul 121-742, Korea
(Received August 12, 1997)

요 약

회수 · 재사용상에 문제가 있는 열경화성 복합재료를 대체하고 우수한 성능을 갖는 다양한 형상의 복합제품을 생산하고자 하는 요구에 부응하여, 최근 끌어당김 성형공정을 이용한 열가소성 장섬유 복합재료의 개발 연구가 활발히 진행되고 있다. 열가소성 장섬유 복합재료를 연속적으로 제조하기 위해서는 높은 점도를 갖는 용융수지를 보강섬유 다발내로 용이하게 함침시킬 수 있는 방법의 개발과 함께 다이의 설계가 가장 중요한 관건이 되고 있으므로, 본 연구에서는 비뉴톤성 거동을 보이는 용융수지의 수직방향 침투도를 예측할 수 있는 반해석적인 모델을 수립함으로써 끌어당김 성형공정의 다이 설계에 이용하고자 하였다. 전단박화 현상이 매우 큰 비뉴톤성 수지가 다공성 섬유매질의 수직 방향으로 침투할 때에 대한 흐름 거동을 유한요소법을 사용하여 미시적 관점에서 해석하고, 거시적 관점의 Darcy 법칙과 결부지음으로써 수직방향의 침투도와 점도의 비로 정의되는 mobility의 변화를 조사하였다. 유량에 대해 무차원화한 비뉴톤성 유체와 뉴톤성 유체의 normalized transverse mobility의 상대적인 비를 power law index에 대해 멱함수의 형태로 축적시킨 다음 환원 충전함량에 대하여 도시한 결과 보강섬유의 배열조건과 유변학적 거동에는 무관하게 단일 선상에 놓임을 확인할 수 있었다. 이로부터 수치해석 결과를 수직방향 침투도와 점도의 영향으로 분리하여 해석하고, 보강섬유의 충전함량과 최대 충전함량을 알게 되면 비뉴톤성 유체의 수직방향 침투도를 용이하게 결정할 수 있는 반해석적인 형태의 개선된 Darcy식을 제시하였다.

Abstracts— In recent years, to solve the problem of recycle and reuse of thermosetting composites, and to satisfy the needs for making of a wide variety of high performance composite products, studies on the development of the long fiber reinforced thermoplastic composites (LFRTPC) have been carried out very actively. A major problem in manufacturing LFRTPC by using pultrusion process is to uniformly and completely impregnate thermoplastic molten resin into the small gaps between the tightly packed reinforcing fibers because of their high viscosity. Hence, understanding of the flow of molten resin through fibrous medium is very important to develop novel methods for impregnation. Moreover, it is impossible for us to design an optimum die without knowing the residence time to impregnate thermoplastic resin into fiber bundle. In response of this need, we have developed a semi-analytic model for predicting the transverse permeability for non-Newtonian fluid flow across arrays of aligned fiber bed. The flow behavior of non-Newtonian fluids with strongly shear thinning character was interpreted by using the finite element method from microscopic viewpoint, and then the transverse mobility, defined as the ratio of permeability and viscosity, of the cell was estimated by using Darcy's law. We found that the scaled ratio of the normalized mobilities of non-Newtonian and Newtonian fluids with respect to the flow rate versus the reduced volume fraction is collapsed on a single line. From this result, the permeability and viscosity values could be separated from the simulation results of non-Newtonian fluids, and a semi-analytic model of modified Darcy's law could be consequently deduced. The transverse permeability and effective viscosity in this model are expressed only as functions of the fiber volume fraction, the ultimate volume fraction to capture the packing structures, and power law index.
Keywords: Non-Newtonian fluid, transverse permeability, normalized mobility, modified Darcy law, semi-analytic model, melt impregnation.

1. Introduction

The use of high performance thermoplastic composites will only increase if efficient and economical processing technique can be developed. Economically, the ideal method for preparing thermoplastic composites is to impregnate the fiber reinforcement directly with high viscous molten resin, and the major challenge is to uniformly and com-

*Present address: Daelim Research Center, Daegeon 305-345, Korea

pletely wet the reinforcement without damaging the fibers.

Thus, one of the most important parameters in composite manufacturing processes is the permeability of the fibrous porous media, because it controls resin penetrating into the fiber bundles, so strongly influence the impregnation property. Moreover, it is impossible for us to design the nice die without knowing the residence time to impregnate thermoplastic molten resin into fiber bundle in manufacturing of thermoplastic long fiber composites by pultrusion process[1].

Newtonian fluid flow through porous media has traditionally been described by the empirical Darcy's law, which relates the fluid flow rate to the pressure gradient, fluid viscosity, and permeability of the porous medium.

$$V_o = \frac{K_y}{\mu_o}\frac{\Delta P}{L} \tag{1}$$

in which V_o is the superficial velocity, the velocity one observes on a macroscopic scale, μ_o is the viscosity of the fluid. $\Delta P/L$ is the pressure gradient in the direction of flow over a characteristic dimension L, K_y and is the permeability of the porous medium. Currently, permeability is most often obtained experimentally by measuring the directional pressure drop-flow rate relationship as a function of volume fraction. However the experiments are difficult and time consuming, because there are still no established standard permeability measurement methods for different fibrous preformed structures. Thus a model for predicting permeability as a function of preformed microstructure would be useful. Such a model would lead to understanding of the structural features that influence the physics of the flow through such materials, and thus potentially enable one to tailor the microstructure such that it has both the desired reinforcing capability and the necessary permeability to fill efficiently.

Several models have been proposed to estimate the value of the permeability for various porous media. The basic approach used to develop such models is to determine the resistance of a viscous fluid to flow in idealized model geometry, and then back calculate the permeability from pressure drop-flow rate relationship. Capillary models such as Kozeny-Carman equation[2,3] are among the earliest models for predicting the permeability of the porous medium based upon an idealized medium structure, which consists of tortuous capillaries. In this approach, the hydraulic radius concept was used to relate the capillary dimensions to the geometric parameters of the porous medium. Its extension to flow across cylinders was carried out by only redefining the hydraulic radius[4-6]. Even though this model has been used successfully for isotropic granular media, it does not work well for either axial or transverse permeability of aligned fibrous media. Bruschke[7] has shown that the results of the capillary model deviate significantly from the numerical solution for the flow across an aligned bed of cylinders.

A more realistic approach to predict the permeability is to consider the geometry as an array of aligned cylinders and to calculate the drag resistance across them. Flow perpendicular to regular cylinder arrays has been analyzed quite extensively by using a number of different mathematical treatments[8-12]. To obtain a closed form solution, extreme arrangements of the fiber spacing have been considered. At low porosities when the cylinders are closely spaced, the lubrication approximation holds and one can solve for the flow rate and pressure drop relationship analytically and obtain an expression for the permeability [13]. For flow perpendicular to cylinders that are widely spaced or at high porosities, Happel[14] and Kuwabara[15] both made a solution by use of the cell model concept. Happel applied a zero shear stress boundary condition at the outer surface of the cell, whereas Kuwabara applied a zero vorticity boundary condition. Experiments[16-19] for the flow through arrays of cylinders at high porosities show good agreement with these solutions.

But it is not possible to obtain an exact solution when one extends these models to generalized Newtonian fluids due to the nonlinear nature of the resulting equations. In the literature there are no analytical studies available for flow past cylinder arrays by use of the cell model but results have been published for flow around spheres. One approach is to linearize the problem about the Newtonian point, and thus arrives at a solution which shows good agreement for slightly shear thinning fluids[20]. Another study uses a stress and velocity variational principle to arrive at a solution for power law fluids[21]. This approach has been extended to Ellis and Carreau model fluids[22, 23]. Based on the lubrication approximation, Bafna and Baird[24] presented the analytical solution for the flow of power law fluids in the gap transverse to reinforcing fibers, and they found the degree of shear thinning of the polymeric melt is very significant on the pressure drop during flow through reinforcement. Lately, Bruschke and Advani [25] proposed a hybrid model by matching two limiting solutions of lubrication approach for low porosities and a cell model solution for high porosities. This model provided a closed form solution that described flow of shear thinning fluids past an array of cylinders over the full

porosity range.

Berdichevsky and Cai[26] proposed an unified model, which is described as a function of the fiber volume fraction and the ultimate volume fraction to capture the fiber assembly status, for estimating the permeability of fibrous media by using self-consistent method. This method considers the flow and energy balance of the insertion of a micro level physical model into a homogeneous medium. Papathanasiou and Lee[27] investigated numerically the effects of micro-structure on the effective transverse permeability of unidirectional arrays of cylindrical fibers using boundary element method. They found that a fully random structure exhibits a permeability slightly higher than a perfect square array for high porosity values for $\phi>0.8$, with this trend disappearing for $\phi<0.8$ and the averages coinciding with the result of the perfect square array.

In this study, we use the finite element simulation for different packing structures to investigate the variation of the permeability or mobility of viscous Newtonian and non-Newtonian fluids. From these numerical results, we also derive the semi-analytic model of modified Darcy's law for the flow of non-Newtonian fluids through regularly spaced fiber arrays. The parameters of this model can be expressed only as a function of power law index, fiber volume fraction and the ultimate fiber volume fraction to capture the fiber assembly status. And we will utilize this model equation to optimal design of a crosshead die for impregnating polymeric melt through the continuous rovings with multiple monofilaments.

2. Theoretical

In many types of fiber reinforcement, the pore geometry is very complicated on a micro level. A more realistic approach to predict the transverse permeability is to consider the geometry as an array of aligned fibers and calculate the drag resistance across them.

2.1. Numerical Solution of the Flow Problem

In-line square, staggered square, rectangular, triangular, and hexagonal arrays are all possible arrangements in an aligned fiber bed. As consolidation of an aligned fiber bed proceeds, the fiber will tend to nest in a way that square arrangements will be changing to staggered square and triangular, and ultimately to a close-packed hexagonal array. Thus, we tried to calculate the transverse permeability by using a representative cell as depicted in Fig. 1, which can describe various types of arrangements only changing

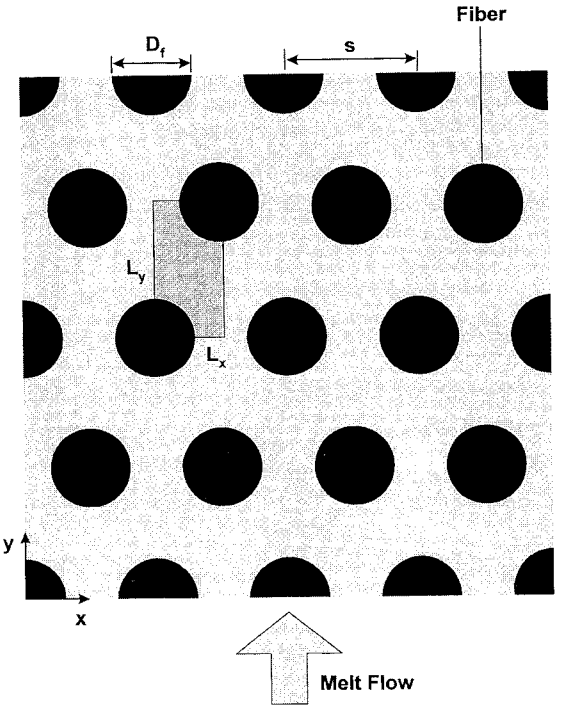

Fig. 1. Representative cell and transverse flow through idealized packing structure of parallel aligned fibers.

cell aspect ratio.

Since the flow around the fibers is assumed in a creeping flow regime, inertial effects were ignored. A numerical flow simulation package, POLYFLOW®, was used to solve the Stokes equation for the truncated power law fluid flow through a given fiber packing array. Constant pressure conditions were applied at the inlet and outlet of the cell. No slip boundary conditions were applied on the fiber surfaces and symmetry conditions were applied on the remaining surfaces. The flow rate was calculated for a prescribed pressure drop and the effective permeability of the cell was estimated using Darcy's law. The porosity was changed by only changing the fiber diameter while keeping the given packing arrangement exactly, and numerical simulations were carried out over a porosity range from 0.05 to 0.95.

To check the periodic condition in the model analysis, we investigate the consistency of transverse velocity profiles at inlet and outlet regions of the two different cell geometries, such as series cell and unit cell in Fig. 2. The Picard iterative procedure is employed to solve the equations and a relative change of less than 0.0001% is utilized as the convergence criterion.

In order to determine the upper bound for which Stokes flow results are adequate, the computed linear and nonlinear solution for flow rate and pressure drop across the

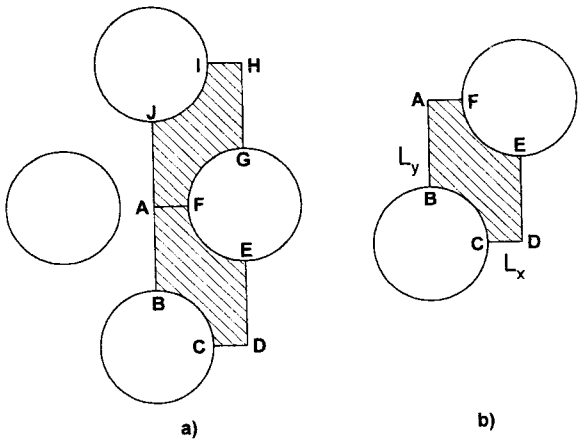

Fig. 2. Two types of cell geometry of hexagonal array for the check of symmetry condition: a) series cell b) unit cell.

cell are compared at different Reynolds numbers. Reynolds number is defined as[28]:

$$R_e = \frac{\rho V_0^{2-n} d}{24\varepsilon H} \tag{2}$$

where ρ and d are the density of fluid, and the gap distance between surfaces of neighborhood fibers. H is viscosity level parameter and is given by:

$$H = \frac{\mu_0}{3}\left(\frac{1+2n}{n}\right)^n\left(\frac{\varepsilon d}{2}\right)^{1-n} \tag{3}$$

Flows corresponding to Reynolds numbers between 10^0 to 10^{-12} are simulated for several packing arrays over entire range of fiber volume fraction.

The results obtained for the flow on the microscopic fiber level are then related to the flow on the macroscopic level that are governed by Darcy's law. The transverse permeability of Newtonian fluid is:

$$K_y = \frac{\int_{A_f} V_y dA_f}{A_t}\frac{\mu_0}{dP/dy} \tag{4}$$

where A_f is the cross sectional area of the fluid flow, and A_t is the total cross sectional area of fluid and fibers. V_y is the transverse velocity of fluid and is calculated by

$$\int_{A_t} V_y dA_f = \sum_{ei=1}^{N_{elem}} \frac{1}{N_{elem}} A_e V_{y,ei} \tag{5}$$

However, it is not possible to separate the permeability and viscosity values from the simulation results for the non-Newtonian fluid flow, since the fluid viscosity varies throughout the unit cell depending on the local strain rates. Therefore, the mobility will be defined as the ratio of the permeability and viscosity. Darcy's law then becomes

$$V_o = M\frac{\Delta P}{L} \tag{6}$$

where M is the mobility of flow in the porous medium. The mobility of non-Newtonian fluid is calculated by using Eqs. 5 and 6:

$$M = \frac{\int_{A_t} V_y dA_f}{A_t}\frac{1}{dP/dy} \tag{7}$$

2.2. Semi-analytic Model

The mobility may be nondimensionalized with respect to the flow rate resulting in a normalized mobility M*,

$$M^* = \frac{\mu_o}{Q^{1-n} r_f^{2n}} M \tag{8}$$

in which Q denotes the flow rate through the unit cell and can be substituted for the fiber space (s) multiplied by the average fluid velocity, Q=sV. The normalized mobility for a given packing array is not dependent on the flow rate and pressure drop, but only dependent on the flow behavior index and porosity. If the porous medium has a constant porosity, the normalized mobility of non-Newtonian fluid with constant flow behavior index has to be kept a constant value regardless of the changes of the flow rate and the fiber radius. And also, as n tends to unity, the normalized mobility reduces to the normalized permeability K_y/r_f^2. This means that the mobility is proportional to $Q^{1-n}r_f^{2(n-1)}$ from Eq. 8.

From the above results, the ratio of M* and $M^*_{Newtonian}$

$$\frac{M^*}{M^*_{Newtonian}} = \frac{\mu_o M/Q^{1-n} r_f^{2n}}{K_y/r_f^2} \tag{9}$$

can be expressed as a function with a power of (1-n). Therefore, if the ratio of M* and $M^*_{Newtonian}$ is taken by the power of 1/(1-n), the scaled ratio of that, $(M^*/M^*_{Newtonian})^{1/(1-n)}$, is only a function of fiber volume fraction as follows:

$$\left(\frac{M^*}{M^*_{Newtonian}}\right)^{1/(1-n)} = f(\phi) \tag{10}$$

where ϕ is the fiber volume fraction. The validity of Eq. 10 was confirmed with the numerical simulation results. Thus, one can separate the effects of the rheology and the porosity of the medium.

From rearranging Eq. 8 for the mobility

$$M = \frac{s^{1-n} V_o^{1-n} r_f^{2n}}{\mu_o} M^* \tag{11}$$

is obtained. Substituting Eq. 11 into Eq. 6 for the macroscopic flow after replacement M* with $M^*_{Newtonian} f(\phi)^{1-n}$ from Eq. 10, we obtain

$$V_o^n = \frac{K_y}{\mu_o [s^{n-1} f(\phi)^{n-1} r_f^{2-2n}]} \frac{\Delta P}{L} \tag{12}$$

where s equals to $\sqrt{\pi(1+S_f^2)/2S_f\phi}\, r_f$. S_f is the cell aspect ratio as shown in Fig. 1.

Through the solution strategy, the final pressure drop-superficial velocity relationship as a function of the porosity for non-Newtonian fluids is:

$$V_o = \frac{K_y}{\mu_{eff}} \frac{\Delta P}{L} \tag{13}$$

where μ_{eff} is an effective viscosity which is expressed as $\mu_o[s^{1-n} f(\phi)^{n-1} r_f^{2-2n}]$. If we introduce the relation between the ultimate fiber volume fraction ϕ_{max} and the cell aspect ratio S_f for a given fiber arrangement, the permeability of Newtonian fluid from Gebart's result[29] is

$$K_y = \frac{a}{4} \left(\sqrt{\frac{\phi_{max}}{\phi}} - 1 \right)^{\frac{5}{2}} D_f^2 \tag{14}$$

and the effective viscosity is also expressed as:

$$\mu_{eff} = \mu_o \left(4\sqrt{\frac{\phi_{max}}{\phi}} \right)^{n-1} [f(\phi)]^{n-1} D_f^{1-n} \tag{15}$$

where D_f is the diameter of fiber. The ϕ_{max} and a are constant with $\pi/2\sqrt{3}$, $16/9\pi\sqrt{6}$ for the hexagonal packing arrangement of fiber, respectively.

The above resulting equations from 13 to 15 are satisfied with the modified Darcy's law for non-Newtonian fluids, and the parameters of these equations can be expressed only as a function of the fiber volume fraction and the ultimate fiber volume fraction to capture the fiber assembly status.

3. Results and Discussions

The numerical results of transverse velocity profiles of a truncated power law fluid flow through a series of cells are summarized in Table 1. In the series cell, the transverse velocity profiles at the inlet and outlet regions of IH, FA,

Table 1. The consistency of transverse velocity profile for hexagonal fiber array at a constant pressure gradient. Power law index of 0.5, power law constant of 10 p, and fiber volume fraction of 0.3 are used

	Coordinate [cm]		V_x [cm/s]		V_y [cm/s]	
	x	y	Series cell	Unit cell	Series cell	Unit cell
IH	1.739e-03	6.023e-03	4.1280e-20		4.4023e-06	
	1.646e-03	6.023e-03	2.0626e-20		4.3874e-06	
	1.554e-03	6.023e-03	2.0311e-20		4.3205e-06	
	1.462e-03	6.023e-03	1.9584e-20		4.1770e-06	
	1.369e-03	6.023e-03	1.8490e-20		3.9332e-06	
	1.277e-03	6.023e-03	1.6674e-20		3.5545e-06	
	1.185e-03	6.023e-03	1.3964e-20		2.9703e-06	
	1.092e-03	6.023e-03	9.3098e-21		1.9803e-06	
	1.000e-03	6.023e-03	0.0000e+00		0.0000e+00	
FA	0.000e+00	3.011e-03	0.0000e+00	0.0000e+00	4.4012e-06	4.4033e-06
	9.230e-05	3.011e-03	-1.9947e-11	0.0000e+00	4.3864e-06	4.3884e-06
	1.847e-04	3.011e-03	-6.3567e-11	1.5200e-20	4.3201e-06	4.3215e-06
	2.770e-04	3.011e-03	-1.2363e-10	0.0000e-00	4.1768e-06	4.1780e-06
	3.693e-04	3.011e-03	-1.9060e-10	1.3882e-20	3.9330e-06	3.9341e-06
	4.617e-04	3.011e-03	-2.6741e-10	0.0000e-00	3.5545e-06	3.5557e-06
	5.540e-04	3.011e-03	-3.3279e-10	1.0452e-20	2.9702e-06	2.9717e-06
	6.464e-04	3.011e-03	-3.2862e-10	0.0000e+00	1.9806e-06	1.9833e-06
	7.387e-04	3.011e-03	0.0000e+00	0.0000e+00	0.0000e+00	0.0000e+00
CD	1.739e-03	0.000e+00	0.0000e+00	0.0000e+00	4.4009e-06	4.4033e-06
	1.646e-03	0.000e+00	0.0000e+00	0.0000e+00	4.3860e-06	4.3884e-06
	1.554e-03	0.000e+00	0.0000e+00	0.0000e+00	4.3188e-06	4.3215e-06
	1.462e-03	0.000e+00	0.0000e+00	0.0000e+00	4.1751e-06	4.1780e-06
	1.369e-03	0.000e+00	0.0000e+00	0.0000e+00	3.9312e-06	3.9341e-06
	1.277e-03	0.000e+00	0.0000e+00	0.0000e+00	3.5529e-06	3.5557e-06
	1.185e-03	0.000e+00	0.0000e+00	0.0000e+00	2.9684e-06	2.9717e-06
	1.092e-03	0.000e+00	0.0000e+00	0.0000e+00	1.9806e-06	1.9833e-06
	1.000e-03	0.000e+00	0.0000e+00	0.0000e+00	0.0000e+00	0.0000e+00

and CD are nearly same within a relative change of less than 0.03%. It is indicated the periodic condition from one cell to a connected cell is kept. Consequently, it can be thought that only the analysis of the unit cell would be guarantee nice results. Moreover, in the unit cell, we can see the transverse velocity profiles of FA and CD is exactly same. Table 2 shows the normalized transverse mobility is very stable in spite of the great change of pressure drops or Reynolds numbers. Therefore, it is known the normalized transverse mobility shown in the equation 6 is very well defined.

Fig. 3 shows the convergence test of the numerical computation for the hexagonal array of the fiber volume fraction of 0.3 by using FEM, with isoparametric-Gaussian quadrature order of 2. The convergence is checked by varying the element number or finite element mesh size. In the lower element numbers the underestimated results are obtained, but beyond an element number the normalized transverse mobility arrives at a steady value independent of power law index. The element number is chosen as a compromise between the solution accuracy and the computation time. So all numerical calculations to obtain the velocity profiles are performed under the choosing element of 360 for the unit cell.

The effects of fiber packing arrangements are also investigated for the case of Newtonian fluid flow. As shown in Fig. 1, the aspect ratio S_f of the representative cell can be varied to obtain the different packing structures. Fig. 4 shows there are the extreme points for the normalized longitudinal permeabilities defined in the Newtonian fluid. For the normalized longitudinal permeability, the minimum value turns up at the cell aspect ratio of the hexagonal packing structure. Inversely, the maximum value of the transverse permeability appears at the region between the square packing and the hexagonal packing. It is explained that with the increase of the value of S_f, the distance between the rows increases but the gap between fibers within the row decreases.

Fig. 5 compares the numerical simulation results for the case of Newtonian fluid flow with the different estimation results. Gebart's estimation results[29] have excellent agreement with the simulation results for both hexagonal array and square array. Gutowski's results[30] have also good agreement with the simulation results for both arrays. SCM

Table 2. The stability of numerical calculation of dimensionless mobility with various pressure drop for for hexagonal fiber array. Power law index of 0.5, power law constant of 10 p, and fiber volume fraction of 0.3 are used

Pressure drop ΔP[dyne/cm^2]	Reynolds number (Re)	Superficial vel. V_o [cm/s]	Mobility M [cm^3/s g]	Normalized Mobility M*
10	0.2097e-10	0.5889e-05	0.1718e-08	0.1244e+00
20	0.1678e-09	0.2355e-04	0.3561e-08	0.1244e+00
30	0.5663e-09	0.5300e-04	0.5342e-08	0.1244e+00
40	0.1342e-08	0.9422e-04	0.7122e-08	0.1244e+00
400	0.1342e-05	0.9422e-02	0.7122e-07	0.1244e+00
40,000	0.1342e+01	0.9422e+02	0.7122e-05	0.1244e+00

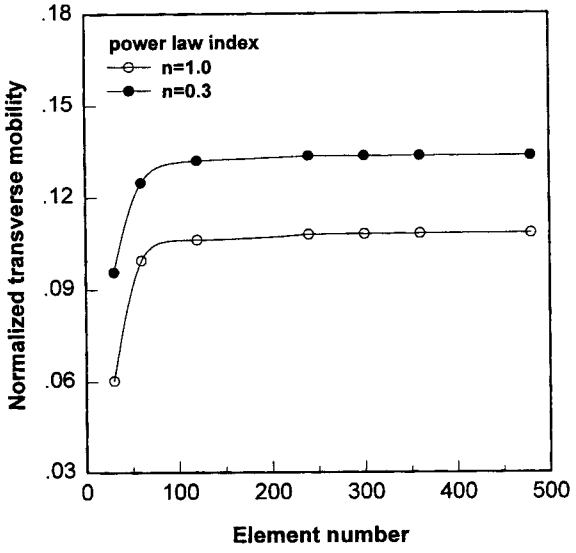

Fig. 3. Convergence test of the numerical computation using FEM with isoparametric-Gaussian quadrature order of 2. Fiber volume fraction is 0.3.

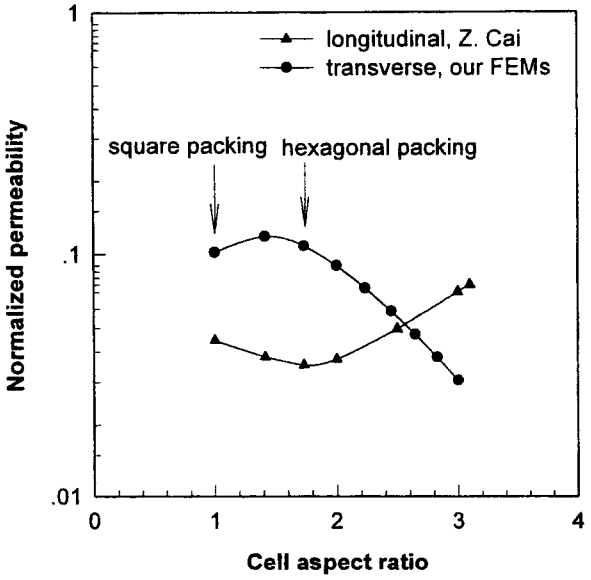

Fig. 4. Comparison of normalized longitudinal and transverse permeability of Newtonian fluid for various cell aspect ratio. Fiber volume fraction is 0.3.

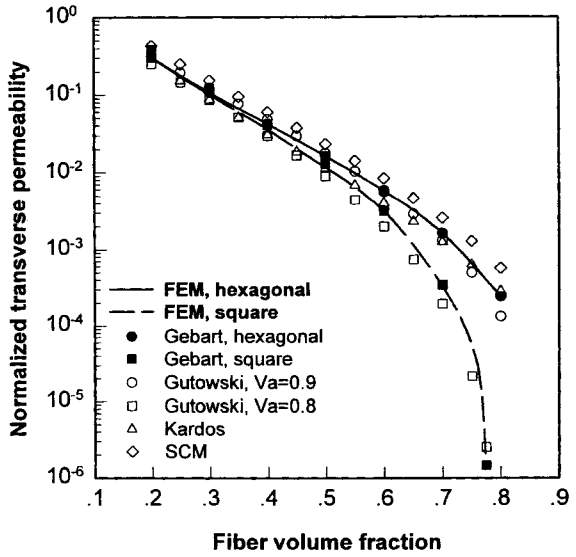

Fig. 5. Comparison of our FEM results and the various estimations on the normalized transverse permeability of Newtonian fluid.

results[26] are similar behavior with the numerical results of hexagonal array, but they are overestimated. At low fiber volume fractions, the predictions by Kardos[31] yield lower values of the normalized permeabilities than the simulation results for both arrays. While at high fiber volume fractions the hexagonal spacing simulation shows relatively good agreement with Kardos results. From Fig. 6, we can see that the agreement between the predictions for flow transverse to regularly aligned fibrous particles and the experimental results[32-45] is good. Only part of the experimental data which many previous workers found turned out to be suitable for inclusion in this study. The fundamental criterion for accepting a set of results is that the data follow Darcy's law. If the data do not follow Darcy's law, then experimental results which the Reynolds number is less than 10 are selected. A second criterion is applied when the experimental fluid is a gas except Bate's results[32]. To ensure that the fluid does not slip at the fiber surface, the Knudsen number is required to be less than 0.01. The diameters of fibrous packing particles ranges over 0.001 μm to 10000 μm. At each medium, the packing fibers is a randomly or non-randomly oriented in planes normal to the flow.

Most polymers show shear thinning behavior as depicted in Fig. 7, which shows the melt viscosity of PP resin at different melt temperatures. The effect of shear rate was corrected by single point method for the viscosity data obtained by plate-plate rheometer (ARES, Rheometrics) at low shear rate regions, and was corrected by Weissenberg-Rabinowitch method for the viscosity data obtained by capillary rheometer (Rheograph 2003, Goettfert) at high shear rate regions. And the entrance effect was corrected by Bagley method.

The shear thinning nature of matrix will play a significant role in the flow of molten resin through fibrous medium. Only with a complete understanding of this impregnation behavior can the novel design of crosshead die, and production efficiency in manufacturing long fiber reinforced thermoplastic composites by pultrusion process be optimized. Thus, the flow behavior of non-Newtonian fluids

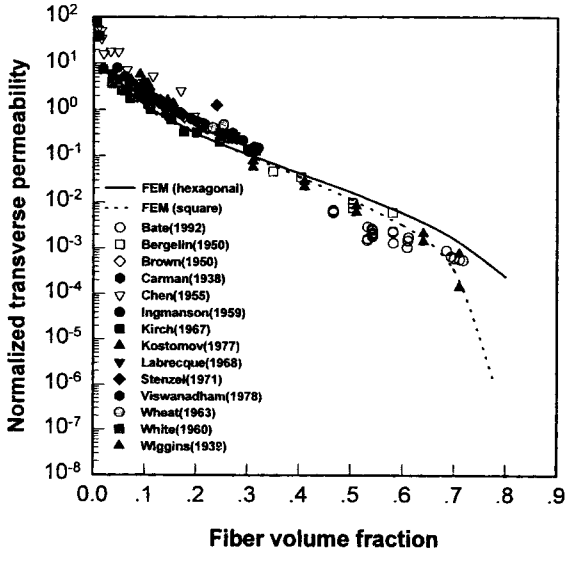

Fig. 6. Comparison of experimental and simulation results for the normalized transverse permeability.

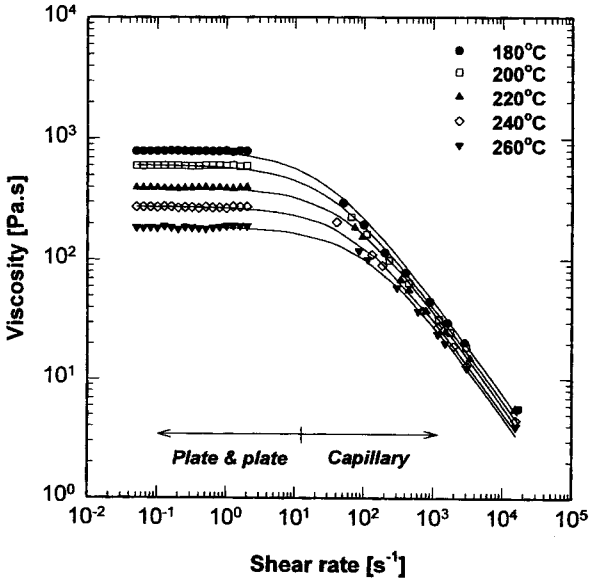

Fig. 7. Shear viscosity as a function of shear rate for polypropylene of MI 30 at various temperatures.

with strong shear thinning character was interpreted by using the finite element method from microscopic viewpoint.

From the numerical simulation results for non-Newtonian fluids, it is not possible to separate the permeability and viscosity values, since the fluid viscosity varies throughout the unit cell depending on the local strain rates. The mobilities, defined as the ratio of permeability and viscosity, for the flow of generalized Newtonian fluids across the hexagonal array of fibers are depicted in Fig. 8. The power law indices are varied from 0.3 to unity, and the power law constant is kept at 10 poise. These results provide insight into the dependence of the mobility on the rheological properties and the fiber volume fraction. We can see that the mobility is more significantly decreased, as the degree of shear thinning of the polymeric melt becomes larger. Especially, it is prominent in the higher fiber volume fraction.

Fig. 9 plots the normalized transverse mobilities of non-Newtonian fluids with respect to the flow rate against the fiber volume fraction. As the power law index decreases for a given flow rate, the average fluid viscosity decreases, and as a result the normalized transverse mobility increases. This means the pressure drop during flow through reinforcement is greatly reduced if the polymeric melt is strongly shear thinning. It also suggests the possible use of additives to promote shear thinning in the polymer matrix in order to impregnate fiber reinforcement with molten resin for a short duration. Consequently, the degree of shear thinning is very important factor in manufacturing long fiber reinforced thermoplastic composites, since the

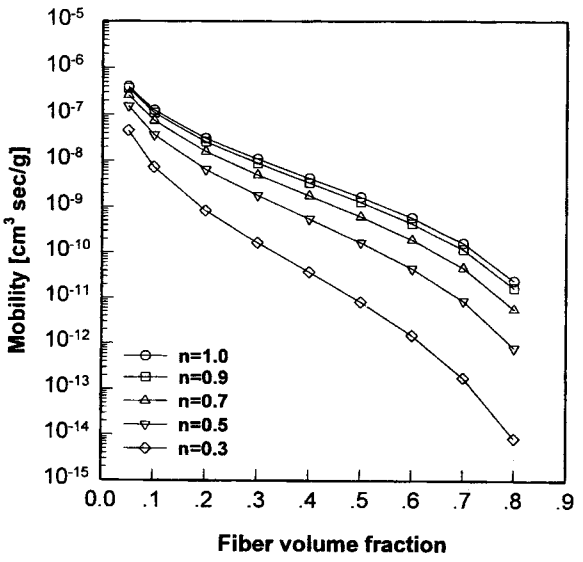

Fig. 8. Mobility versus fiber volume fraction for the flow of power-law fluids across a hexagonal array of fibers.

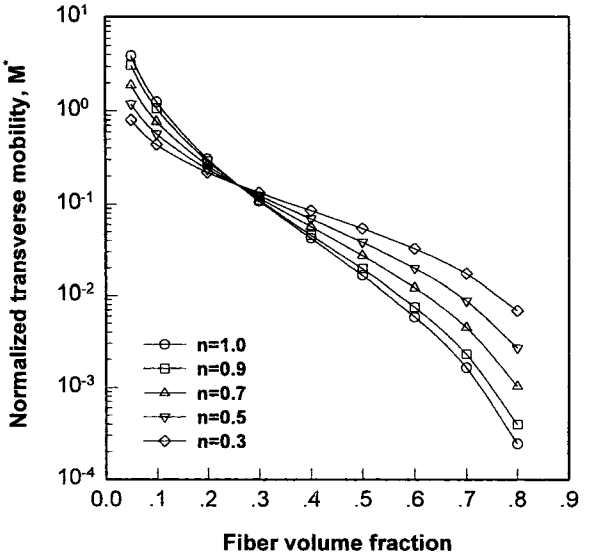

Fig. 9. Normalized transverse mobility versus fiber volume fraction for the flow power-law fluids across a hexagonal array of fibers.

real pultrusion process is generally operated with the higher fiber volume fractions above 0.25, and directly impregnated fiber rovings with molten resin.

In the case of a Newtonian fluid, the permeability can be simply separated from the mobility. To separate the effects of rheology and porosity from the mobility of non-Newtonian fluids, the ratio of the normalized transverse mobilities of Newtonian fluid and non-Newtonian fluids is scaled as a function of the power law index. And the scaled ratios for the hexagonal and square fiber arrays are plotted against the fiber volume fraction in Fig. 10. The scaled ratio of normalized transverse mobilities is collapsed on a single line regardless of power law index. Thus, we can separate the effects of the rheology and the fiber volume fraction from the mobility of non-Newtonian fluids. Still the scaled ratio of normalized transverse mobilities shows clearly that even with the same fiber volume fraction, there are considerable variations because of the packing structures. These results indicate that characteristics of a fiber bundle other than fiber volume fraction are needed to correctly describe the permeability status of a fiber assembly. The scaled ratios of the normalized mobilities for different fiber packing structures are replotted against the reduced fiber volume fraction as shown in Fig. 11. Also we found that the results are collapsed on a single line regardless of the fiber packing structures. This result indicates that the scaled ratio of the normalized mobilities is presented only a function of the reduced fiber volume fraction.

From these results, the permeability and viscosity values

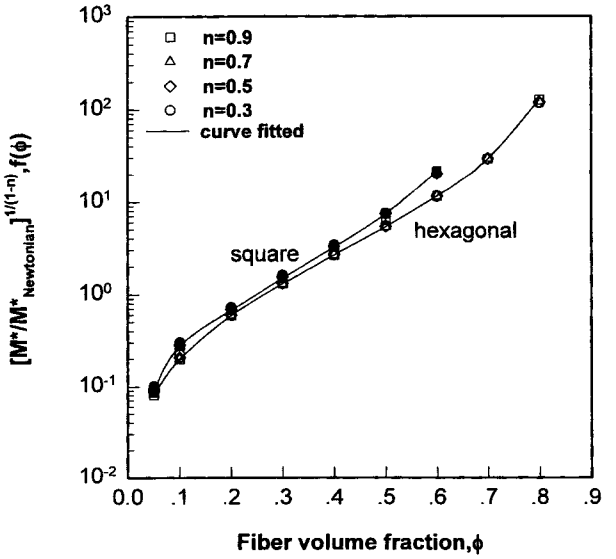

Fig. 10. Curve fit of the scaled ratio of normalized transverse mobilities as a function of fiber volume fraction for the flow of power-law fluids through hexagonal and square fiber arrays.

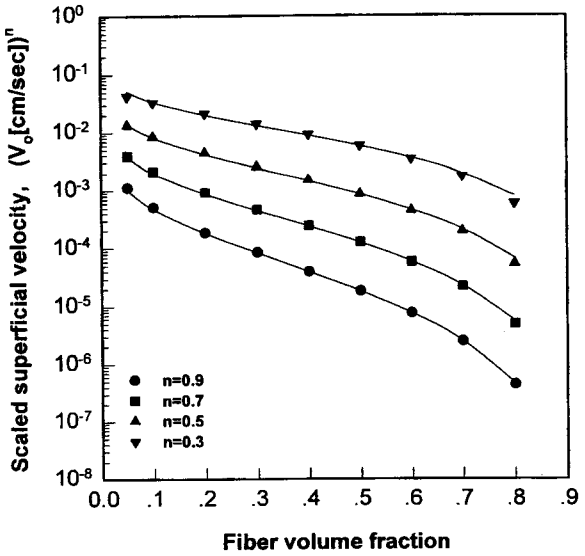

Fig. 12. Comparison of the semi-analytic results and the simulation results for power-law fluids across a hexagonal array of fibers. Solid lines denote FEM simulation results and symbols denote the semi-analytic results with power-law index of 0. 9, 0.7, 0.5 and 0.3, respectively.

can be separated from the simulation results of non-Newtonian fluids, and a semi-analytic model of modified Darcy's law can be consequently deduced. The transverse permeability and effective viscosity in this model are expressed only as a function of the fiber volume fraction, the ultimate volume faction to capture the packing structures, and power law index. Fig. 12 shows the comparison the closed form solution of semi-analytic model with the simulation results for power law fluids across a hexagonal fiber array. Over the full range of the fiber volume fraction and even in the strong shear thinning, the semi-analytic results show great agreement with the simulated results.

The main advantages of this semi-analytic model are very easy to apply to real state independent of the fiber packing arrays if only one determines the ultimate fiber volume fraction for any fiber beds, and to obtain the solutions for the wide range of the degree of shear thinning.

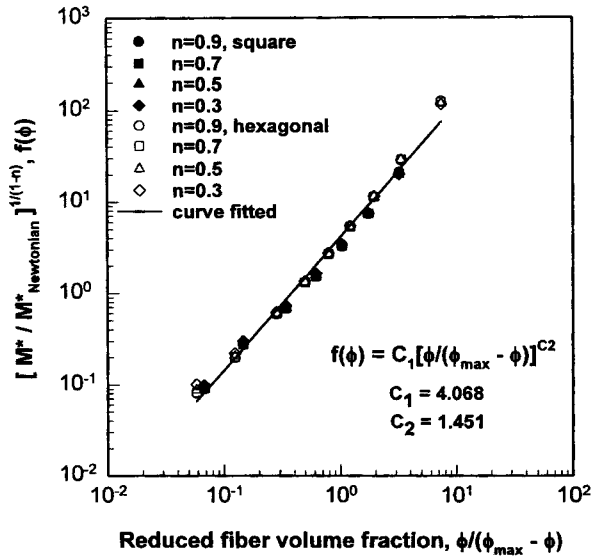

Fig. 11. Scaled ratio of normalized transverse mobilities as a function of reduced fiber volume fraction for the flow of power-law fluids through hexagonal and square fiber arrays.

4. Conclusions

A major problem in manufacturing LFRTPC by using pultrusion process is to uniformly and completely impregnate the small gaps between the tightly packed reinforcing fibers with thermoplastic molten resin because of their high viscosity. Hence, understanding of the flow of molten resin through fibrous medium is very important to develop novel methods for impregnation.

Numerically obtained transverse permeabilities of aligned fiber beds for Newtonian fluids agree with various estimation results, especially well with Gebart's result. All the presented successful reproduction of published experimental observations is presented.

The flow behavior of non-Newtonian fluids with strong shear thinning character is interpreted by using the finite element method from the microscopic viewpoint, and then the transverse mobility, defined as the ratio of permeability

and viscosity, of the cell was estimated by using Darcy's law. From these results, we found that as the power law index decreases for a given flow rate, the normalized transverse mobility increases. This indicates the pressure drop during flow through reinforcement is greatly reduced if the polymeric melt is strongly shear thinning. It also suggests the possible use of additives to promote shear thinning in the polymer matrix in order to impregnate fiber reinforcement with molten resin for a short duration.

Also we found that the scaled ratio of the normalized mobilities of non-Newtonian and Newtonian fluids with respect to the flow rate versus the reduced volume fraction is collapsed on a single line regardless of the fiber packing arrays and power law index. The permeability and viscosity values could be separated from the simulation results of non-Newtonian fluids, and a semi-analytic model for predicting the transverse permeability for non-Newtonian fluid flow across arrays of aligned fiber bed could be consequently deduced. The transverse permeability and effective viscosity in this model are expressed only as functions of the fiber volume fraction, the ultimate volume faction to capture the packing structures, and power law index.

The validity of this semi-analytic model equation was confirmed from comparing with the numerical results. It is ascertained that the results of the semi-analytic model were in good agreement over the full porosity range with those of the numerical simulation for all possible arrangements in an aligned fiber bed and the very wide shear thinning region. And this model equation will be utilized to optimal design of a crosshead die for impregnating polymeric melt through the continuous rovings with multiple monofilaments.

Nomenclatures

A_f : the cross sectional area of the fluid flow
A_t : the total cross sectional area of fluid and fibers
d : the gap distance between surfaces of neighborhood fibers
D_f : diameter of fiber
H : viscosity level parameter defined by Eq. 3
K_y : transverse permeability of Newtonian fluid
L : characteristic length
M : mobility defined as the ratio of permeability and viscosity
M* : normalized transverse mobility
$M^*_{Newtonian}$: normalized transverse mobility of Newtonian fluid
n : flow behavior index of power law fluid
r_f : radius of fiber
Q : volumetric flow rate
s : the fiber space between the centers of fibers
S_f : the cell aspect ratio
V_o : superficial velocity
V_y : transverse velocity of the fluid
y : transverse direction coordinate

Greek letters

ΔP : pressure drop
ε : porosity
ϕ : fiber volume fraction
ϕ_{max} : ultimate fiber volume fraction to capture the packing structure
μ : viscosity of the non-Newtonian fluid
μ_{eff} : effective viscosity
μ_o : zero shear rate viscosity
ρ : density of the fluid

Acknowledgment

This paper was supported in part by NON-DIRECTED RESEARCH FUND, Korea Research Foundation.

References

1. J.S. Lee and J.W. Lee, ANTEC SPE, **42**, 2536 (1996).
2. J. Kozeny, *Sitzungsberichte Wiener Akadmie der Wissenschaft,* **Abt Iia 136**, 272 (1927).
3. P.C. Carman, *Trans. Inst. Chem. Eng,* **15** 150 (1937).
4. R.C. Lam and J.L. Kardos, *ANTEC, SPE,* **35**, 1408 (1989).
5. T. Dave, J.L. Kardos and M.P. Dudukovic, *Polym. Comp.,* **8**, 123 (1987).
6. J.G. Williams, C.E.M. Morris and B.C. Ennis, *Polym. Eng. Sci.,* **14**, 413 (1974).
7. M.V. Bruschke, Ph.D. Thesis, University of Delaware 1992.
8. L. Skartis and J.L. Kardos, *ACS 5th,* **5**, 548 (1990).
9. C. Chiemlewski, C.A. Petty and K. Jayaraman, *ACS 5th,* **5**, 557 (1990).
10. T.G. Gutowski, T. Morigaki and Z. Cai, *J. Comp. Mater.,* **21**, 172 (1987).
11. A.S. Sangaini and A. Acrivos, *Int. J. Multiphase Flow,* **8**, 193, 343 (1982).
12. J.E. Drummond and M.I. Tahir, *Int. J. Multiphase Flow,* **10**, 515 (1984).
13. J.B. Keller, *J. Fluid Mech.,* **18**, 94 (1964).
14. J. Happel, *AIChE J.,* **5**, 174 (1959).
15. S. Kuwabara, *J. Phys. Soc. Japan,* **14**, 527 (1959).
16. C. Chiemlewski, C.A. Petty and K. Jamaraman, *ACS 5th,* **5**, 557 (1990).
17. A.A. Kirsch and N.A. Fuchs, *Ann. Occupational Hygiene,* **10**, 23 (1967).
18. G.W. Jackson and D.F. James, *Can. J. Chem. Eng.,* **64**, 364 (1986).
19. L. Skartis, B. Khomami and J. Kardos, *J. Rheol.,* **36**, 589 (1992).

20. Y. Kawase and J.J. Ulbrecht, *Chem. Eng. Sci.,* **36**, 1193 (1981).
21. V. Mohan and Raghuraman, *AIChE J.,* **21**, 805 (1975).
22. V. Mohan and Raghuraman, *Int. J. Multiphase Flow,* **2**, 581 (1976).
23. R.P. Chhabra and J.R. Raman, *Chem. Eng. Commun.,* **27**, 23 (1984).
24. S.S. Bafna and D.G. Baird, *J. Comp. Mater.,* **26**, 683 (1992).
25. M.V. Bruschke and S.G. Advani, *J. Rheol.* **37**, 479 (1993).
26. A.L. Berdichevsky and Z. Cai, *Polym. Comp.,* **14**, 132 (1993).
27. T.D. Papathanasiou and P.D. Lee, *Polym. Comp.,* **18**, 242 (1997).
28. S. Vossoughi and F.A. Seyer, *Can. J. Chem. Eng.,* **52**, 666 (1974).
29. B.R. Gebart, *J. Comp. Mater.,* **26**, 1100 (1992).
30. T.G. Gutowski, Z. Cai, S. Bauer, D. Boucher, J. Kingery and S. Wibenab, *J. Comp. Mater.,* **21**, 650 (1987).
31. R.C. Lam and J.L. Kardos, *Proc. Am. Soc. Comp., 3rd Tech. Conf.,* 3, Seattle (1988).
32. P.J. Bate, H. Ripert and J.M. Charrier, *ANTEC, SPE,* **38**, 1709 (1992).
33. O.P. Bergelin, G.A. Brown, H.L. Hull and F.W. Sullivan, *Trans. ASME,* 881 (1950).
34. J.C. Brown Jr., *TAPPI,* **33**, 130 (1950).
35. P.C. Carman, *Soc. Chem. Ind.,* **57**, 225 (1938).
36. C.Y. Chen, *Chem. Rev.,* **55**, 595 (1955).
37. W.L. Ingmanson, B.D. Andrews and R.C. Johnson, *TAPPI,* **42**, 840 (1959).
38. A.A. Kirsch and N.A. Fuchs, *Ann. Occupational Hygiene,* **10**, 23 (1967).
39. A.G. Kostornov and M.S. Shevchuk and M.S. Poroshkovaya, *Metallurgiya,* **9**, 50 (1977).
40. R.P. Labrecque, *TAPPI,* **51**, 8 (1968).
41. K.H. Stenzel, A.L. Rubin, W. Yamayoshi, T. Miyata, T. Suzucki, T. Sohde and M. Nishizawa, *Trans. Am. Soc. Artif. Int. Organs,* **17**, 293 (1971).
42. R. Viswanadham, D.C. Agrawal and E.J. Kramer, *J. Appl. Phys.,* **13**, 725 (1942).
43. J.A. Wheat, *Can. J. Chem. Eng.,* **41**, 67 (1963).
44. M.L. White, *J. Phys. Chem.,* **64**, 1563 (1960).
45. E.J. Wiggins, W.B. Campbell and O. Maass, *Can J. Research,* **17**, Sec.B 318 (1939).
46. A.E. Scheidegger, *Physics of Flow through Porous Media,* 3rd ed., University of Toronto Press 1974.
47. J. Happel and H. Brenner, *Low Reynolds Number Hydrodynamics: Mechanics of Fluids and Transport Processes,* Martinus Nijhof 1986.
48. S. Ranganathan, F.R. Phelan Jr. and S.G. Advani, *Polym. Comp.,* **17**, 222 (1996).
49. P. Simacek and S.G. Advani, *Polym. Comp.,* **17**, 887 (1996).
50. Y.-N. Lai, B. Khomami and J.L. Kardos, *Polym. Comp.,* **18**, 368 (1997).